

IEEE SENSORS 2026

Rotterdam, Netherlands || October 25–28, 2026

Radar-based Sparsity-aware Dynamic Occupancy Grid Mapping

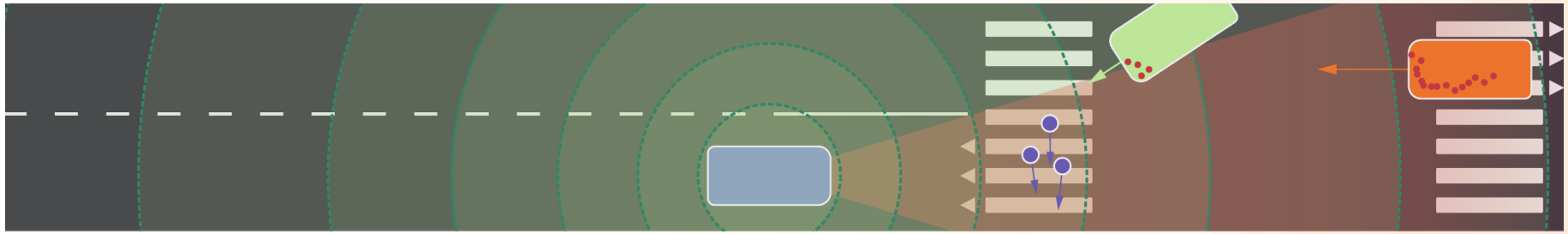
Peiyuan Zhai[1], Mingdong Dai[1], Geethu Joseph[1], Nitin Jonathan Myers[1], Ashish Pandharipande[2]

[1] Delft University of Technology, The Netherlands [2] NXP Semiconductors, The Netherlands

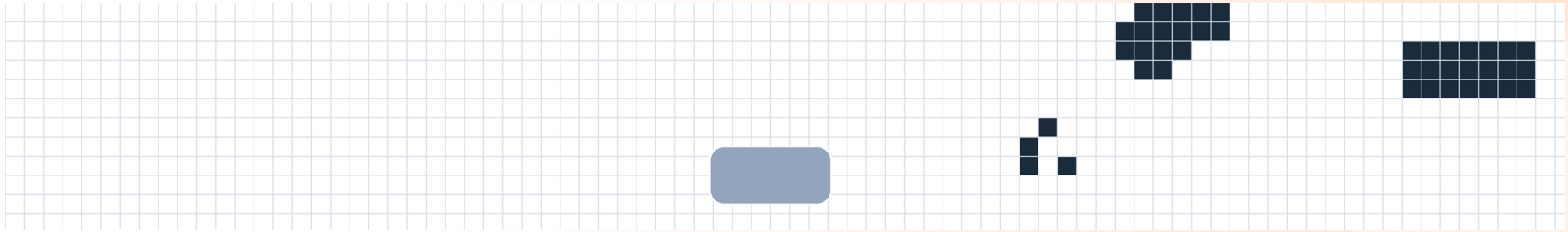
TU Delft | NXP

What is occupancy grid mapping?

Scene



Occupancy grid map



Each cell

Free

$x_n \approx 0$

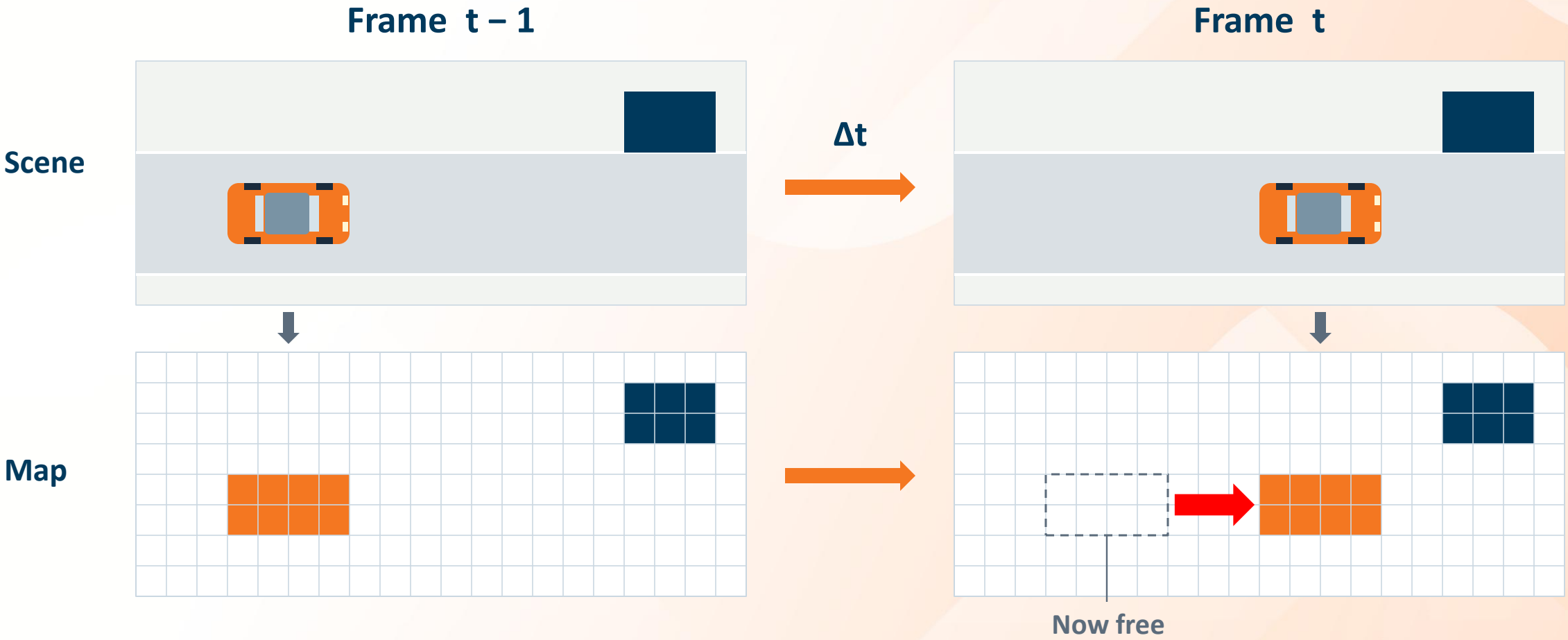
Occupied

$x_n \approx 1$

Each cell stores its occupancy probability $x_n \in [0, 1]$.

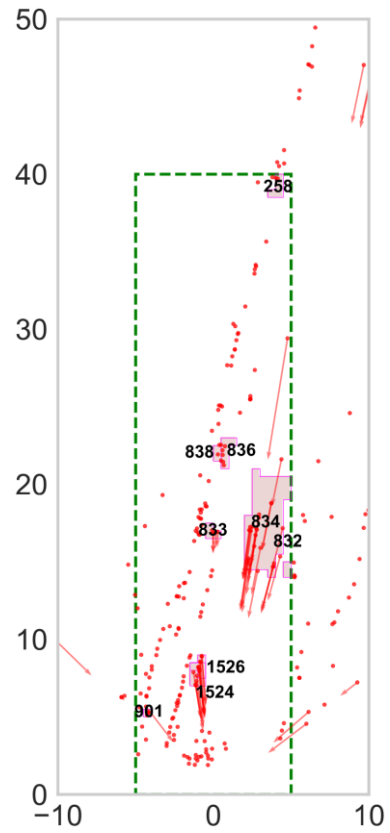
Dynamic occupancy grid mapping

Occupied cells change as objects move



IEEE SENSORS 2026
Rotterdam, Netherlands || October 25-28, 2026

Radar data



Radar points + Doppler arrows, VoD [4]

Strengths

- Works in rain, fog and darkness
- Doppler velocity for every point

Challenges

- Sparse points
- Clutter and multipath cause false alarms

Radar: temporal structure through Doppler

Doppler information tells us some knowledge of how obstacles move.

Map: spatial structure through obstacle clustering

Obstacles appear as small clusters of occupied cells, not as isolated points.

Our approach: exploit **both** structures for better reconstruction.

[4] A. Palffy et al., IEEE RA-L, 2022 (View-of-Delft)

Dynamic OGM: where existing methods fall short

Method family	Temporal	Spatial	Sparsity	Remarks
Bayesian occupancy filters [9]–[11]	✓	limited	✗	Temporal model via motion tracking; little spatial modelling
Kernel / GP occupancy maps [12]–[16]	✓	✓	✗	Spatio-temporal kernels; high computational cost
Sparsity-aware OGM (PCSBL) [5]	✗	✓	✓	Static maps; single frame only
This work (DL1 / DL2-PCSBL)	✓	✓	✓	Dynamic PSI inside the sparse Bayesian prior

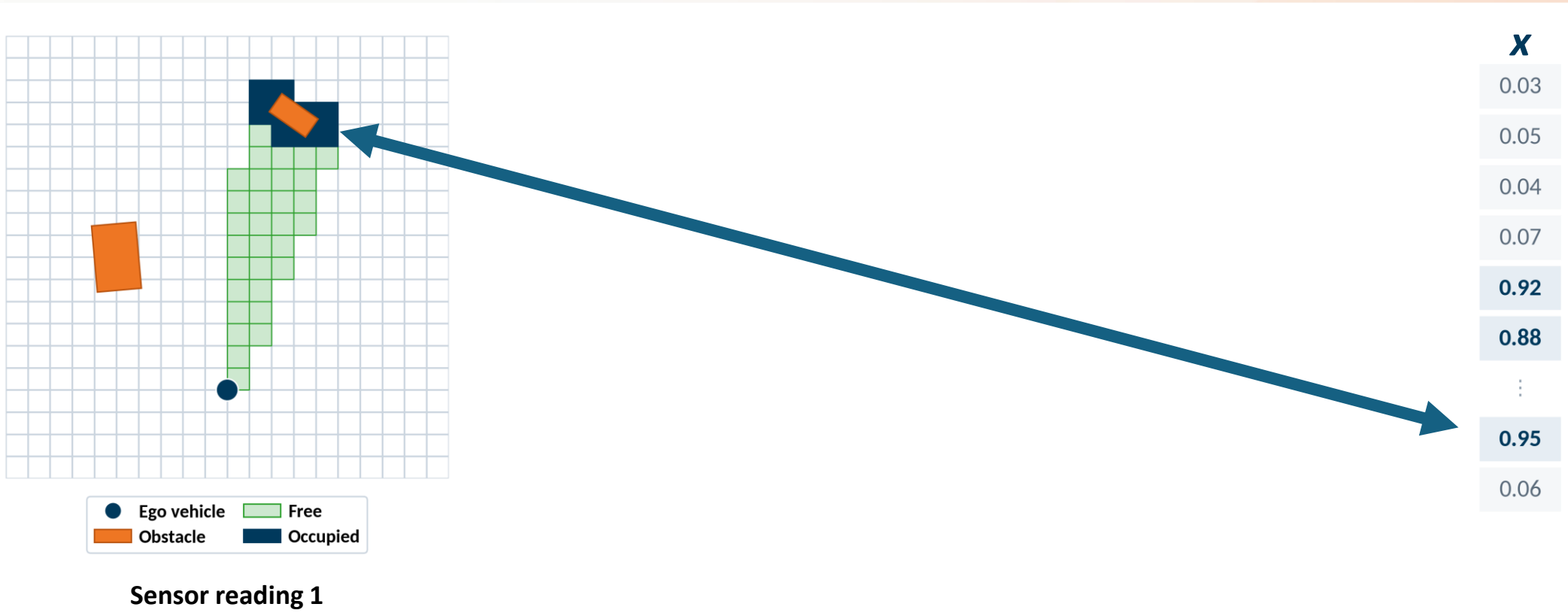
Goal: keep the sparsity and spatial coupling of PCSBL, and add the temporal continuity that radar Doppler makes available.

[5] Ç. Önen et al., 2024 [9] C. Coué et al., 2006 [10] A. Nègre et al., 2014 [11] M. P. Ronecker et al., 2024 [12] S. T. O'Callaghan & F. T. Ramos, 2012 [13] F. Ramos & L. Ott, 2016 [14] K. Doherty et al., 2017 [15] S. T. O'Callaghan & F. T. Ramos, 2016 [16] R. Senanayake & F. Ramos, 2017

From radar points to a sparse recovery problem

A linear measurement model is required.

Each radar reading is turned into linear measurements of the occupancy probabilities, so the map can be found by sparse recovery.



[5] Ç. Önen et al., IEEE Sens. J., 2024

From radar points to a sparse recovery problem

A linear measurement model is required.

Each radar reading is turned into linear measurements of the occupancy probabilities, so the map can be found by sparse recovery.

Vectorized probability map



Sensor reading 1

y	1	2	3	4	5	6	⋯	N−1	N
≈ 0	**1**	**1**	**1**	0	0	0	⋯	0	0
≈ 1	0	0	0	0	**1**	**1**	⋯	0	0

Sensor reading 1

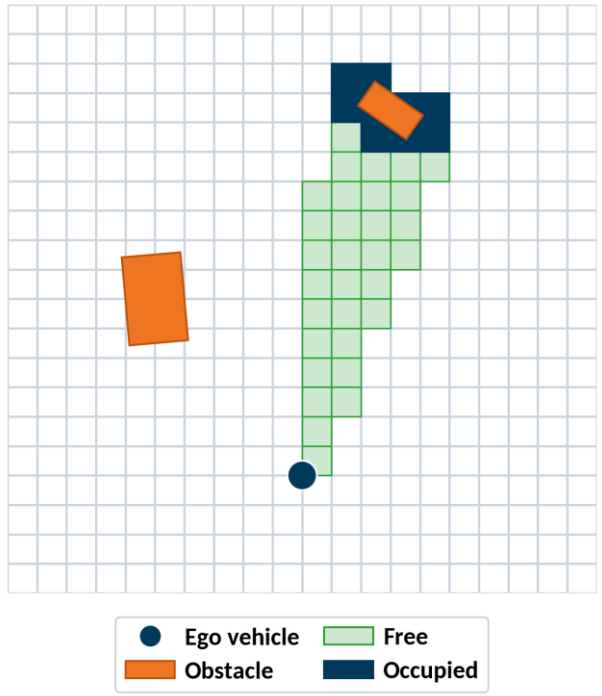
x
0.03
0.05
0.04
0.07
0.92
0.88
⋮
0.95
0.06

- **Record indices of detected cells in rows**
- **These multiplications add up the occupancy probabilities from free or occupied cells**

[5] Ç. Önen et al., IEEE Sens. J., 2024

From radar points to a sparse recovery problem

A linear measurement model is required. Each radar reading is turned into linear measurements of the occupancy probabilities, so the map can be found by sparse recovery.



Sensor reading 1

Vectorized probability map

y	1	2	3	4	5	6	⋯	N−1	N
≈ 0	**1**	**1**	**1**	0	0	0	⋯	0	0
≈ 1	0	0	0	0	**1**	**1**	⋯	0	0

Sensor reading 1

Record the occupancy status

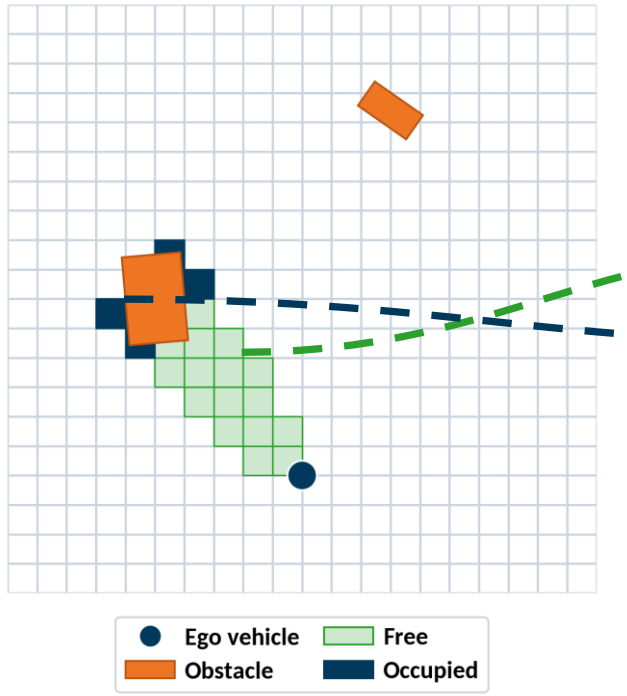
Sensor readings encoded in the rows

x
0.03
0.05
0.04
0.07
0.92
0.88
⋮
0.95
0.06

[5] Ç. Önen et al., IEEE Sens. J., 2024

From radar points to a sparse recovery problem

A linear measurement model is required. Each radar reading is turned into linear measurements of the occupancy probabilities, so the map can be found by sparse recovery.



Sensor reading 2

Vectorized probability map

y	1	2	3	4	5	6	⋯	N−1	N		x
≈ 0	1	1	1	0	0	0	⋯	0	0	Sensor reading 1	0.03
≈ 1	0	0	0	0	1	1	⋯	0	0	Sensor reading 1	0.05
≈ 0	0	1	1	1	0	0	⋯	0	0	Sensor reading 2	0.04
≈ 1	0	0	0	0	0	0	⋯	1	0	Sensor reading 2	0.07
											0.92
											0.88
											⋮
											0.95
											0.06

Iterate through all the points

[5] Ç. Önen et al., IEEE Sens. J., 2024

From radar points to a sparse recovery problem

Stacking all readings gives y = A x + n. The map x is sparse, so recovering x from y is a sparse recovery problem.

y measurement labels
(≈ 0 free, ≈ 1 occupied)

A spatial coverage of measurements (0/1)

x unknown occupancy probabilities (sparse)

n noise and model mismatch

Vectorized probability map

	y	1	2	3	4	5	6	⋯	N−1	N		x
Sensor reading 1	≈ 0	1	1	1	0	0	0	⋯	0	0		0.03
	≈ 1	0	0	0	0	1	1	⋯	0	0		0.05
												0.04
Sensor reading 2	≈ 0	0	1	1	1	0	0	⋯	0	0		0.07
	≈ 1	0	0	0	0	0	0	⋯	1	0		0.92
												0.88
		⋮	⋮	⋮	⋮	⋮	⋮	⋮	⋮	⋮		⋮
Sensor reading M	≈ 0	1	0	0	1	0	0	⋯	0	1		0.95
	≈ 1	0	0	0	0	0	1	⋯	0	0		0.06

$$\mathbf{y} = \mathbf{A}\,\mathbf{x}$$

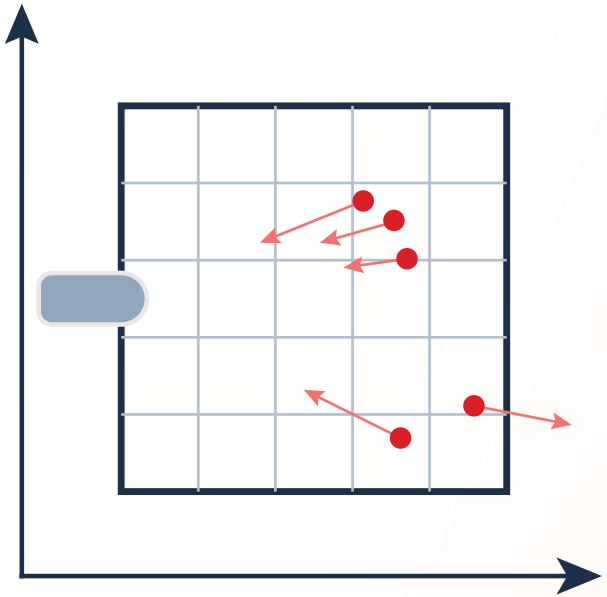
[5] Ç. Önen et al., IEEE Sens. J., 2024

Building dynamic PSI

Prior support information (PSI) predicts likely occupied cells

1 Select moving points

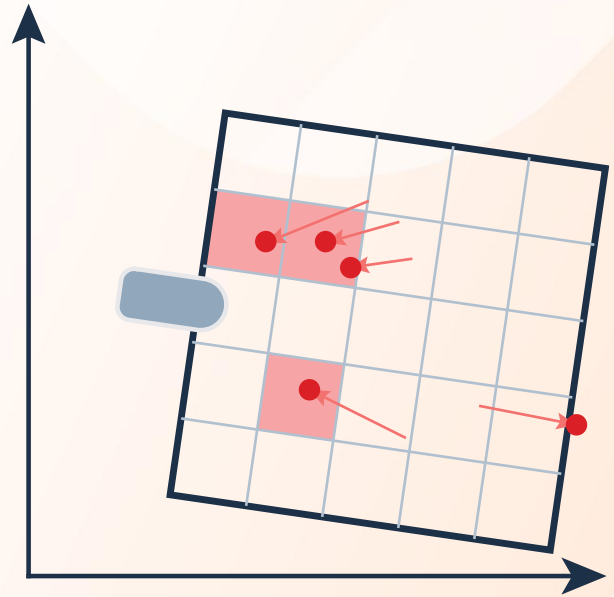
Previous frame $t - 1$



Ego-compensated Doppler
$|v_r| > 1$ m/s

2 Predict current cells

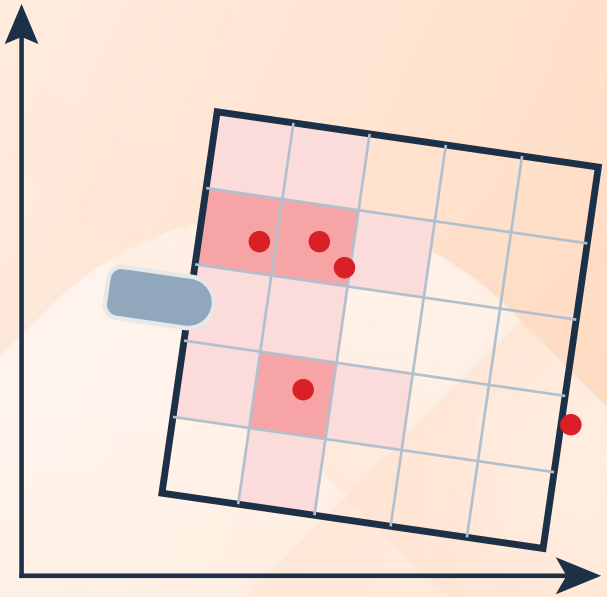
Current frame t



Shift by $v_r \Delta t$
Correct for ego motion

3 Add spatial support

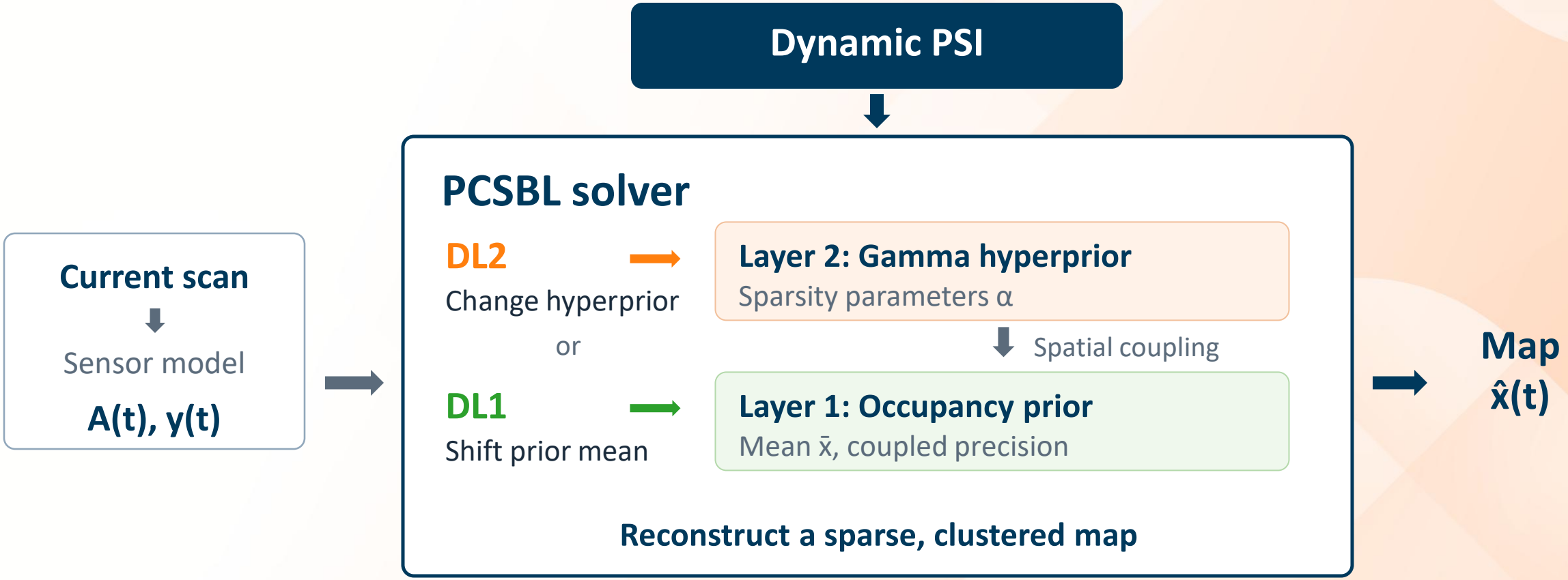
Dynamic PSI



Retain in-grid cells
Include spatial neighbours

Dynamic PSI in the PCSBL solver

PSI can guide either layer of the hierarchical prior

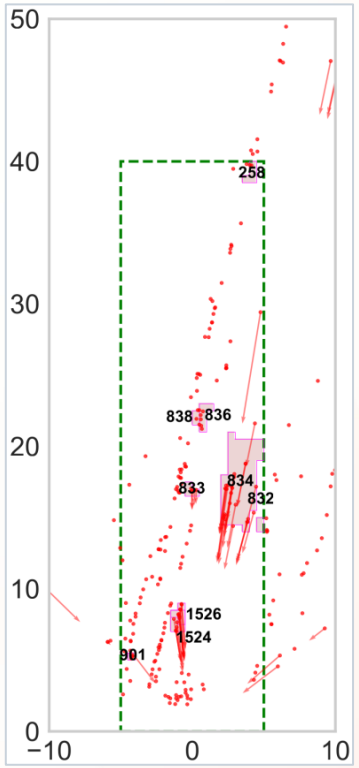


Current measurements can correct errors in the PSI.

Turning scene: frame 965



(a) Camera image



(b) Radar points

Pink: ground-truth boxes.

Numbers: object IDs.

Data: View-of-Delft [4]

Object ID	DBOF	PCSBL	DL2-PCSBL	DL1-PCSBL
#258	0.000	**0.250**	**0.250**	**0.250**
#832 *static*	0.000	0.000	0.000	0.000
#833	0.000	0.000	**0.667**	0.333
#834	0.017	0.052	**0.190**	0.103
#836 *static*	0.000	0.000	0.000	0.000
#838 *static*	0.000	0.000	0.000	0.000
#901 *static*	**1.000**	0.000	0.000	0.000
#1524	0.286	0.000	**0.429**	**0.429**
#1526	**0.333**	0.000	**0.333**	**0.333**
Detected ↑	4 / 9	2 / 9	**5 / 9**	**5 / 9**
AS-NMSE ↓	0.171	0.092	**0.025**	0.031

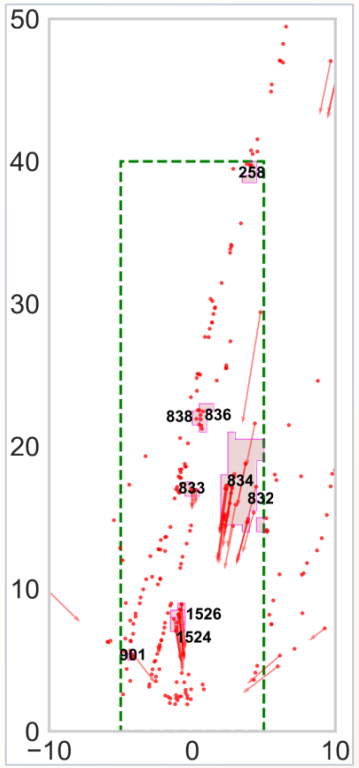
[4] A. Palffy et al., IEEE RA-L, 2022 (View-of-Delft)

Turning scene: frame 965

RESULTS



(a) Camera image



(b) Radar points

Pink: ground-truth boxes.

Numbers: object IDs.

Data: View-of-Delft [4]

Object ID	DBOF	PCSBL	DL2-PCSBL	DL1-PCSBL
#258	0.000	0.250	0.250	0.250
#832 *static*	0.000	0.000	0.000	0.000
#833	0.000	0.000	0.667	0.333
#834	0.017	0.052	0.190	0.103
#836 *static*	0.000	0.000	0.000	0.000
#838 *static*	0.000	0.000	0.000	0.000
#901 *static*	1.000	0.000	0.000	0.000
#1524	0.286	0.000	0.429	0.429
#1526	0.333	0.000	0.333	0.333
Detected ↑	4 / 9	2 / 9	5 / 9	5 / 9
AS-NMSE ↓	0.171	0.092	0.025	0.031

[4] A. Palffy et al., IEEE RA-L, 2022 (View-of-Delft)

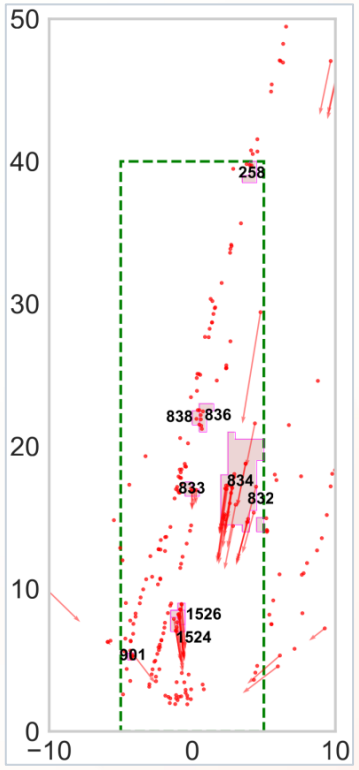
IEEE SENSORS 2026 Rotterdam, Netherlands | October 25-28, 2026

Turning scene: frame 965

RESULTS



(a) Camera image



(b) Radar points

Pink: ground-truth boxes.

Numbers: object IDs.

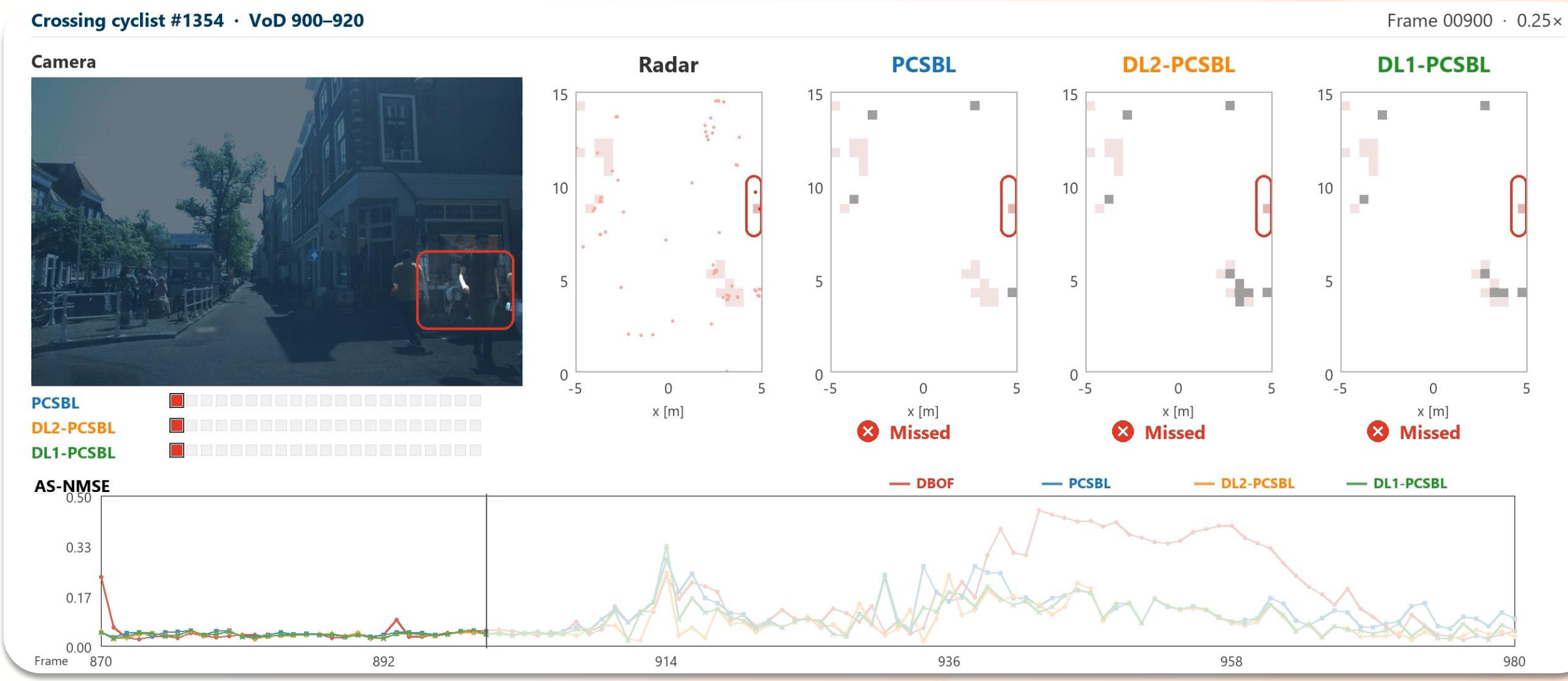
Data: View-of-Delft [4]

Object ID	DBOF	PCSBL	DL2-PCSBL	DL1-PCSBL
#258	0.000	**0.250**	**0.250**	**0.250**
#832 *static*	0.000	0.000	0.000	0.000
#833	0.000	0.000	**0.667**	0.333
#834	0.017	0.052	**0.190**	0.103
#836 *static*	0.000	0.000	0.000	0.000
#838 *static*	0.000	0.000	0.000	0.000
#901 *static*	**1.000**	0.000	0.000	0.000
#1524	0.286	0.000	**0.429**	**0.429**
#1526	**0.333**	0.000	**0.333**	**0.333**
Detected ↑	4 / 9	2 / 9	**5 / 9**	**5 / 9**
AS-NMSE ↓	0.171	0.092	**0.025**	0.031

[4] A. Palffy et al., IEEE RA-L, 2022 (View-of-Delft)

Improved dynamic target detection

RESULTS



Pink: ground-truth boxes.

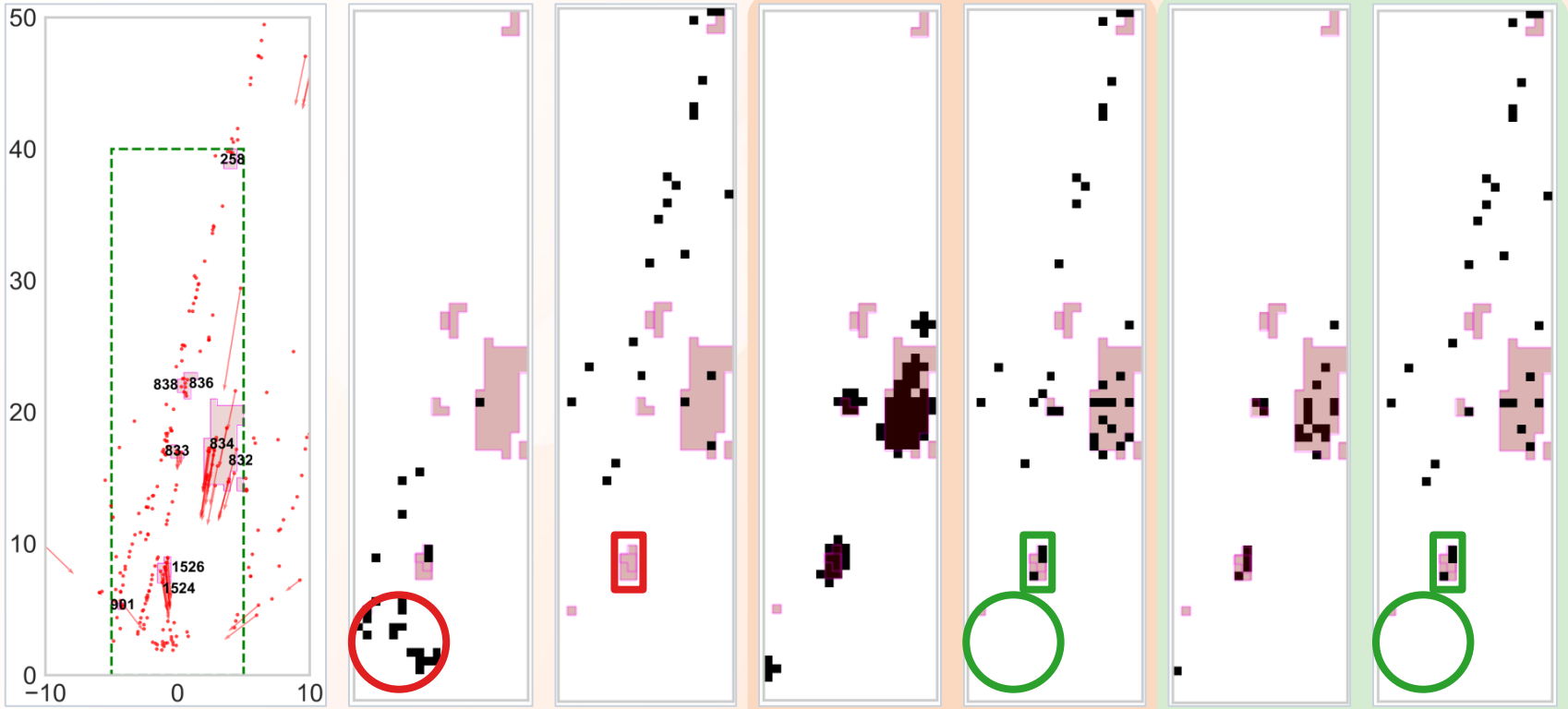
Reduced false alarm



(a) Camera image

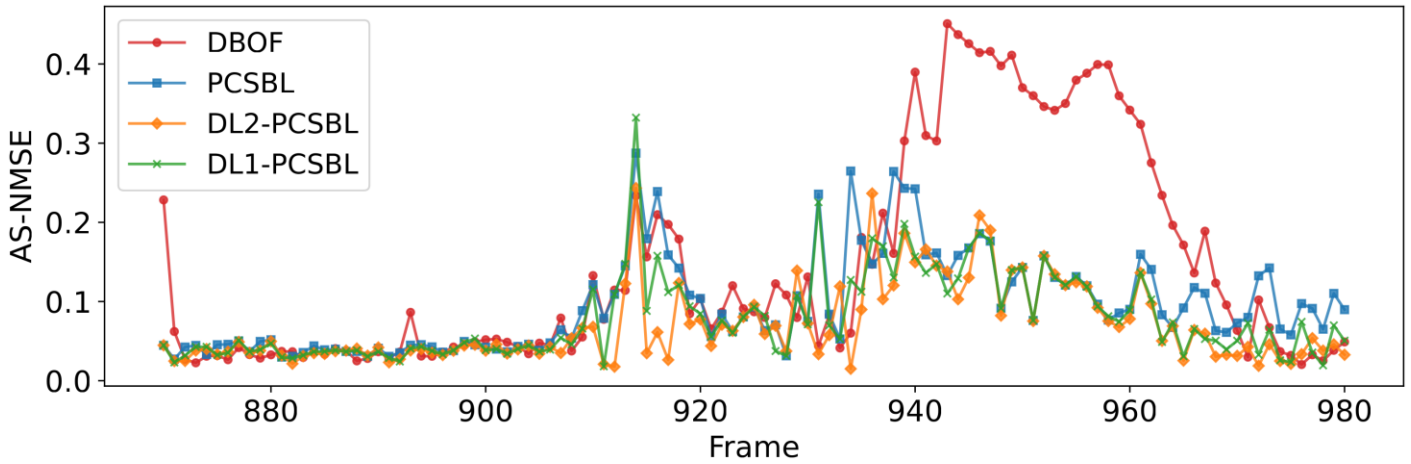
Pink: ground-truth boxes. Black: occupied cells. Numbers: object IDs.

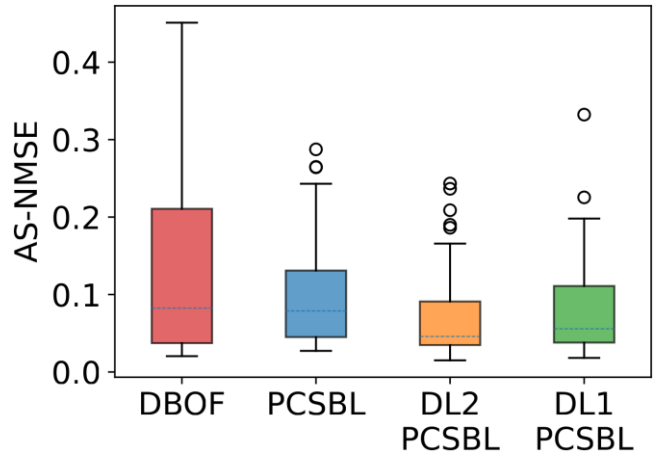
- Target missed (cyclist 1524 / 1526)
- Target detected
- False alarms (static clutter)
- No false alarms here

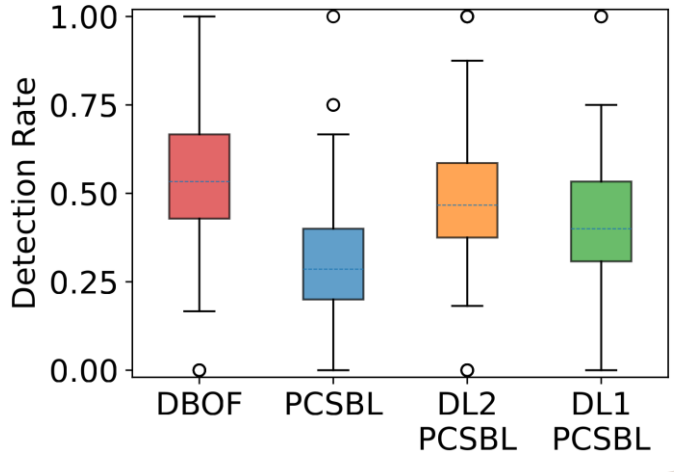


(b) Radar points (c) DBOF (d) PCSBL (e) DL2 PSI (f) DL2 map (g) DL1 PSI (h) DL1 map

Turning scene: frames 870–980







Median over the sequence

AS-NMSE ↓

DBOF	PCSBL	DL2	DL1
0.082	0.079	0.046	0.056

Detection rate ↑

DBOF	PCSBL	DL2	DL1
0.533	0.286	0.467	0.400

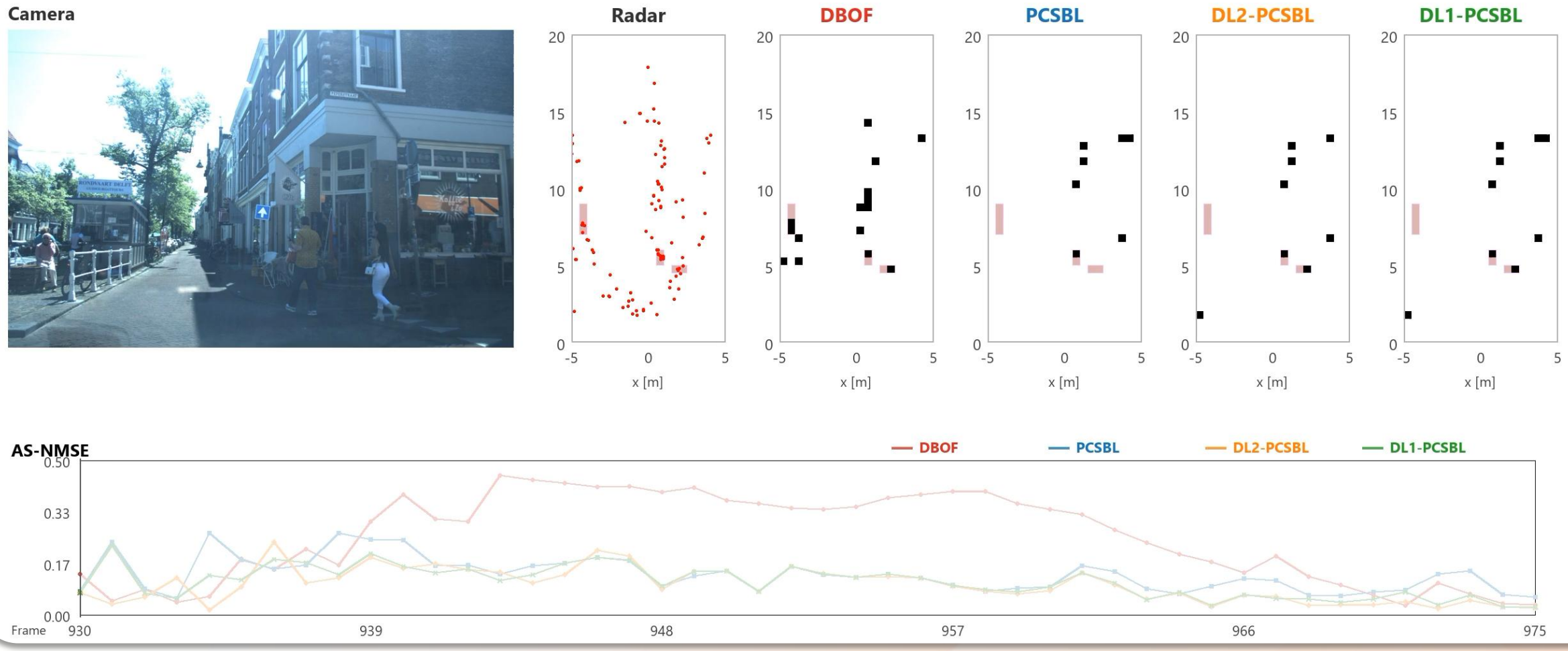
DBOF finds more objects but keeps static clutter: see its AS-NMSE peak in frames 939–969.

Turning scene: frames 870–980

RESULTS

Turning scene · VoD 930–975

Frame 00930 · 0.5×



Pink: ground-truth boxes.

References

[4] A. Palffy, E. A. I. Pool, S. Baratam, J. F. P. Kooij, and D. M. Gavrila, “Multi-class road user detection with 3+1D radar in the View-of-Delft dataset,” IEEE Robot. Autom. Lett., vol. 7, no. 2, pp. 4961–4968, 2022.

[5] Ç. Önen, A. Pandharipande, G. Joseph, and N. J. Myers, “Occupancy grid mapping for automotive driving exploiting clustered sparsity,” IEEE Sens. J., vol. 24, no. 7, pp. 9240–9250, 2024.

[7] J. Fang, Y. Shen, H. Li, and P. Wang, “Pattern-coupled sparse Bayesian learning for recovery of block-sparse signals,” IEEE Trans. Signal Process., vol. 63, no. 2, pp. 360–372, 2015.

[9] C. Coué, C. Pradalier, C. Laugier, T. Fraichard, and P. Bessière, “Bayesian occupancy filtering for multitarget tracking: An automotive application,” Int. J. Robot. Res., vol. 25, no. 1, pp. 19–30, 2006.

[10] A. Nègre, L. Rummelhard, and C. Laugier, “Hybrid sampling Bayesian occupancy filter,” in Proc. IEEE Intell. Veh. Symp., 2014, pp. 1307–1312.

[11] M. P. Ronecker, M. Schratter, L. Kuschnig, and D. Watzenig, “Dynamic occupancy grids for object detection: A radar-centric approach,” in Proc. IEEE Int. Conf. Robot. Autom., 2024, pp. 13991–13997.

[12] S. T. O’Callaghan and F. T. Ramos, “Gaussian process occupancy maps,” Int. J. Robot. Res., vol. 31, no. 1, pp. 42–62, 2012.

[13] F. Ramos and L. Ott, “Hilbert maps: Scalable continuous occupancy mapping with stochastic gradient descent,” Int. J. Robot. Res., vol. 35, no. 14, pp. 1717–1730, 2016.

[14] K. Doherty, J. Wang, and B. Englot, “Bayesian generalized kernel inference for occupancy map prediction,” in Proc. IEEE Int. Conf. Robot. Autom., 2017, pp. 3118–3124.

[15] S. T. O’Callaghan and F. T. Ramos, “Gaussian process occupancy maps for dynamic environments,” in Experimental Robotics, Springer Tracts in Advanced Robotics, vol. 109. Cham: Springer, 2016, pp. 791–805.

[16] R. Senanayake and F. Ramos, “Bayesian Hilbert maps for dynamic continuous occupancy mapping,” in Proc. Conf. Robot Learn., PMLR, vol. 78, 2017, pp. 458–471.

Radar-based Sparsity-aware Dynamic Occupancy Grid Mapping

Dynamic PSI

Previous-frame Doppler predicts likely occupied cells.

Two prior designs

DL1 shifts the prior mean.
DL2 changes the hyperprior.

Results on View-of-Delft

More detections than single-frame PCSBL.
Lower free-space error than both baselines.

Thank you! Questions?

Scan to see more about our research. Slides available.

Peiyuan Zhai · p.zhai@tudelft.nl



IEEE SENSORS 2026

Rotterdam, Netherlands || October 25–28, 2026

Thank you!

Peiyuan Zhai · p.zhai@tudelft.nl

Radar-based Sparsity-aware Dynamic Occupancy Grid Mapping